Int. J. Heat Mass Transfer. Vol. 36, No. 8, pp. 2105–2114, 1993
Printed in Great Britain

0017–9310/93 $6.00 + 0.00

Hot spot locations and temperature distributions in a forced convection photochemical reactor

FALIN CHEN
Institute of Applied Mechanics, National Taiwan University, Taipei, Taiwan 10764, R.O.C.

and

ARNE J. PEARLSTEIN
Department of Mechanical and Industrial Engineering, University of Illinois at Urbana-Champaign, 1206 West Green Street, Urbana, IL 61801, U.S.A.

(*Received* 22 *May* 1992 *and in final form* 30 *September* 1992)

Abstract—We have computed steady axisymmetric temperature distributions in a tubular photoreactor in which fluid in laminar flow absorbs light from an azimuthally uniform, radially incident light source. In addition to the primary on-axis temperature maximum, a second hot spot forms off the centerline as the optical density γ increases. This results from a shift of light absorption toward the wall, which is held at a fixed temperature (e.g. by forced convection cooling on the outside). At still larger γ the centerline hot spot disappears, leading to a decrease in the maximum temperature and accompanied by an increase in the temperature near the wall. There is a critical value of γ, depending on the Peclet number Pe, below which the hot spot is located on the centerline and above which a second hot spot forms and moves off the centerline. The reduction in maximum centerline temperature may be advantageous for product selectivity and yield in the central core of the reactor, but may be disadvantageous with respect to the formation of light-absorbing deposits on the interior of the tube wall. Axial heat conduction has significant effects for $Pe < 50$, including displacement of the hot spot upstream from the exit plane of the illuminated section, as well as an increase in the maximum temperature.

1. INTRODUCTION

A NUMBER of chemical processes are conducted in fluid-phase photochemical reactors. These include small-scale batch syntheses of pharmaceuticals and fine chemicals (e.g. vitamins A and D_3), the 145 000 ton/year manufacture of the nylon-6 and nylon-12 monomers caprolactam and lauryl lactam, and the disinfection of wastewater [1–7].

A critical feature of any photochemical reaction is the inherent nonhomogeneity of the reaction rate (cf. [8]), due to attenuation of light by absorption as it passes through the reactor. Since heat generation in a photochemical reactor, whether due to nonradiative processes following photon absorption or exothermic reactions following the primary process, is a consequence of light absorption, the temperature distributions in such reactors are also inherently nonuniform [9].

In many photochemical systems, undesired thermal reactions compete with the photochemical reaction(s) of interest, resulting in reduced product yield and selectivity along with increased byproduct formation [10 (p. 582), 11–14]. The temperature dependence of the rates of the thermal reactions is typically of the Arrhenius form

$$\text{Rate} \sim \exp(-E_a/RT) \quad (1)$$

so that good temperature control is essential if the rates of side reactions having significant activation energies are to be minimized [3, 10 (p. 649), 11, 15]. Examples include many photochlorination reactions, in which the competing thermal and photochemical mechanisms lead to different product distributions [16].

No less important an objective of thermal control in liquid- and gas-phase photoreactors is to minimize formation of wall deposits, which usually reduce light intensity in the reactor [3, 17–22]. These deposits arise from chemisorption, condensation, or adsorption of free radicals or other reactive intermediates produced in the primary photochemical event following light absorption, or of nonvolatile products. Condensation/evaporation and adsorption/desorption rates are usually sensitive to the temperature at and near the wall, as are the rates of secondary decomposition reactions which wall deposits may undergo. Wall deposit formation has been a problem in at least one commercialized photochemical reaction, having been reported in the process development program leading to large-scale photochlorination of cyclohexane to cyclohexanone oxime [3, 21], a key step in the synthesis of the nylon-6 monomer, caprolactam.

Thus, the determination of temperature distributions, maximum temperatures, and hot spot

NOMENCLATURE

a	average energy degraded to heat per photon absorbed
A_n, B_n, C_n	expansion coefficients in equations (6a–c)
c_p	specific heat
C_A	concentration of photosensitizer A
E_a	activation energy
$H_n(\xi)$	eigenfunction of equations (8a–c)
I_0	incoming light intensity at tube wall $r = r_0$
J_n	integral defined in equation (9)
k	thermal conductivity
L	length of illuminated region
Pe	Peclet number, $U_0 r_0 \rho c_p / k$
$Q(r)$	internal heating rate due to light absorption
r	radial coordinate
R	universal gas constant
r_0	tube radius
T	temperature
T_i	temperature of region i
T_0	temperature of tube wall
U_0	centerline fluid velocity
z	axial coordinate.

Greek symbols

γ	optical density, $\mu C_A r_0$
δ_{ij}	Kronecker delta
ε	molar extinction coefficient
η	dimensionless axial coordinate, $z/(r_0 Pe)$
θ_i	dimensionless temperature in region i
θ_{fd}	fully developed dimensionless temperature distribution
λ_n	eigenvalue of equations (8a–c)
μ	$\varepsilon \ln 10$
ξ	dimensionless radial coordinate, r/r_0
ρ	fluid density
σ	aspect ratio of illuminated region 2, L/r_0.

locations is of considerable importance in the design, optimization, and operation of photochemical reactors. Despite a general recognition of the importance of thermal control in photochemical reactors [3, 10 (pp. 582, 649), 11, 23, 24], including the possibility of overheating, ignition, and explosion [3, 16, 25], very little is known about temperature distributions in photochemical systems.

With the exception of our earlier brief report [26], previous work on heat transfer in photochemical reactors has focused on the causes and prevention of natural convection in unmixed batch reactors [9, 27–40] of interest to physical chemists, rather than on the prediction of temperature distributions in continuous flow reactors of engineering interest. There is also a large literature concerned with the experimental and theoretical determination of light intensity distributions in photoreactors (cf. refs. [14, 41]).

In this work, we consider heat transfer in laminar flow tubular photoreactors, which have been a popular choice for laboratory studies of kinetics and scale-up [18–20, 42–49], and have also been proposed for large-scale use in production of fuels and other materials in solar photochemical systems [23, 24]. The present work concentrates on temperature distributions, hot spot locations, and maximum temperatures, with particular emphasis on the influence of the optical density of the absorbing fluid.

2. MODEL AND GOVERNING EQUATIONS

We consider photochemical reactions in which light is absorbed by a sensitizer. Two factors motivate the choice of photosensitized reactions in this work. First, these reactions have been studied in the photochemical engineering literature (cf. refs. [49–51]) and are of interest in connection with photopolymerizations and other industrially important processes [51, 52]. Second, the assumptions that only the sensitizer absorbs radiation (i.e. that the reactant(s) and product(s) do not absorb) and that the photosensitizer is not consumed ensure that the energy balance can be decoupled from the species balances. Thus, this relatively simple model allows for detailed analysis of and insight into the basic heat transfer processes in the reactor. More complicated models, incorporating state-of-the-art treatments of the radiation field [14] coupled to the mass balances appropriate to the kinetics of nonsensitized (direct) photochemical reactions, would yield a set of nonlinear three-dimensional partial integro–differential equations, solution of which would require a fully numerical treatment that would not allow for the detailed exploration of reactor thermal behavior possible with our simpler model.

Specifically, we consider steady Poiseuille flow of a Newtonian fluid containing a photosensitizer A at concentration C_A in a long optically transparent circular tube of radius r_0. The fluid enters an illuminated section of length L (region 2 in Fig. 1) where A absorbs radially incident light. The molar extinction coefficient ε of A (which absorbs radiation but is not destroyed by photochemical or thermal processes) is taken as a constant for all wavelengths absorbed. (We can equivalently assume that only one wavelength is absorbed.) We also assume that the reactant(s) and product(s) of the photosensitized reaction do not absorb at the wavelength(s) of interest. Finally, we assume that the density, viscosity, thermal conductivity, and specific heat of the fluid, as well as the

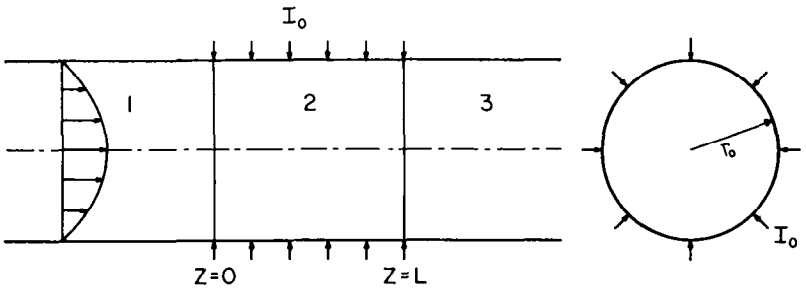

FIG. 1. Geometry of the laminar flow tubular photochemical reactor.

molar extinction coefficient of A, are independent of temperature and composition. With these assumptions, the steady energy equation is

$$\rho c_p U_0\left(1-\frac{r^2}{r_0^2}\right)\frac{\partial T_i}{\partial z}=k\left\{\frac{1}{r}\frac{\partial}{\partial r}\left[r\frac{\partial T_i}{\partial r}\right]+\frac{\partial^2 T_i}{\partial z^2}\right\}+\delta_{i2}Q(r) \quad (2)$$

where T_i is the temperature in region i, $Q(r)=a\mu C_A I(r)$ is the rate at which absorbed energy is converted to heat,

$$I(r)=\frac{2I_0 r_0}{r}e^{-\mu C_A r_0}\cosh(\mu C_A r) \quad (3)$$

is the light intensity within the reactor, a is the average energy ultimately degraded to heat per photon absorbed, $\mu=\varepsilon \ln 10$, and I_0 is the light intensity (power/area) entering the illuminated region. The Kronecker delta in (2) arises because heating is confined to region 2. In (2), we have neglected viscous dissipation heating; we have retained the axial conduction term due to its importance in some of the previous experimental work, as described in Sections 4 and 5. The thermochemical interpretation of a in terms of radiative and nonradiative molecular energy transfer processes (e.g. collisional deactivation and internal conversion) and exothermic reactions has been discussed by Pearlstein [9].

The radial incidence model (3) is a simple approximation to the light intensity distribution in real photoreactors [14] and has been used in a number of studies of the effects of convective and diffusive mixing in tubular reactors [42, 44–47], where its qualitative validity is now well established [14]. This model of the light intensity distribution serves as a good starting point for the analysis of heat transfer in photochemical reactors.

We take the boundary condition at the tube wall to be one of fixed temperature

$$T(r_0,z)=T_0, \quad -\infty<z<\infty \quad (4)$$

corresponding, for instance, to a thin tube wall and very good forced convection cooling (or heating) of the outer surface of the tube. An example of the approximate realization of this boundary condition is found in the work of Matsuura *et al.* [20], in which heated air was passed through an annular quartz jacket surrounding the tubular photoreactor.

The assumption of laminar flow is consistent with the experimental work of Matsuura *et al.* [20] in which the photolysis of acetone was studied in a circular tube photoreactor with a Reynolds number (based on tube diameter, average velocity, and an estimate of the He–acetone viscosity according to standard methods [53 (p. 24)] of 3.1, as well as with the experimental work of Dolan *et al.* [43] in which a large part of an extensive study of the photodecomposition of hexachloroplatinic acid in a circular tube photoreactor was conducted under laminar flow conditions. Consideration of a tube of infinite length is not a serious restriction in light of the Peclet numbers and aspect ratios used in the previous experimental work (see Section 4.2).

3. ANALYSIS

Introducing the nondimensionalization

$$r=\xi r_0 \quad z=\eta r_0 Pe \quad \gamma=\mu C_A r_0$$

$$Pe=U_0 r_0 \rho c_p/k \quad T_i=T_0+\frac{2aI_0 r_0}{k}\theta_i$$

(2)–(4) become

$$(1-\xi^2)\frac{\partial\theta_i}{\partial\eta}=\frac{1}{\xi}\frac{\partial}{\partial\xi}\left(\xi\frac{\partial\theta_i}{\partial\xi}\right)+\frac{1}{Pe^2}\frac{\partial^2\theta_i}{\partial\eta^2}+\delta_{i2}\frac{\gamma e^{-\gamma}\cosh(\gamma\xi)}{\xi} \quad (5a)$$

$$\theta_i(1,\eta)=0 \quad (5b)$$

$$\lim_{\eta\to-\infty}\frac{\partial\theta_1(\xi,\eta)}{\partial\eta}=\lim_{\eta\to\infty}\frac{\partial\theta_3(\xi,\eta)}{\partial\eta}=0 \quad (5c)$$

where $i=1$, 2, and 3. We require the temperature to be bounded everywhere.

We represent the solution of (5a–c) by eigenfunction expansions in regions 1–3, supplemented by the fully developed solution in region 2:

$$\theta_1(\xi,\eta)=\sum_{n=-\infty}^{-1}A_n H_n(\xi)e^{\lambda_n\eta} \quad \eta<0 \quad (6a)$$

$$\theta_2(\xi,\eta)=\sum_{n=-\infty}^{\infty}B_nH_n(\xi)\,e^{\lambda_n\eta}+\theta_{fd}(\xi)\quad 0<\eta<\frac{\sigma}{Pe} \tag{6b}$$

$$\theta_3(\xi,\eta)=\sum_{n=1}^{\infty}C_nH_n(\xi)\,e^{\lambda_n\eta}\quad \frac{\sigma}{Pe}<\eta. \tag{6c}$$

Here, σ is the aspect ratio of the illuminated region and

$$\theta_{fd}(\xi)=e^{-\gamma}\int_{\xi}^{1}\frac{\sinh(\gamma x)}{x}dx \tag{7}$$

is the fully developed solution of 5(a, b) in region 2, which will be approached for sufficiently large σ.

The eigenfunctions $H_n(\xi)$ and eigenvalues λ_n satisfy

$$\frac{d^2H_n}{d\xi^2}+\frac{1}{\xi}\frac{dH_n}{d\xi}+\lambda_n\left[\frac{\lambda_n}{Pe^2}-(1-\xi^2)\right]H_n(\xi)=0 \tag{8a}$$

$$H_n(0)\text{ bounded} \tag{8b}$$

$$H_n(1)=0. \tag{8c}$$

For sufficiently large Pe the axial conduction term in (5a) and (8a) can be dropped, and (8a–c) reduce to a Sturm–Liouville problem. For smaller Pe (e.g. about 2.5 in the experimental work of Matsuura *et al.* [20], based on the tube diameter, average velocity, and estimates of the He–acetone thermophysical properties according to standard methods [53 (pp. 24, 258)], the axial conduction term must be retained, and so the eigenvalue problem (8a–c) is no longer of Sturm–Liouville type.

However, it is well known from previous work on forced convection problems with no internal heating that (8a–c) admit both positive (denoted by $n\leqslant -1$) and negative ($n\geqslant 1$) eigenvalues [54], which are real [55]. The corresponding eigenfunctions are complete [56] and orthogonal with respect to a properly chosen inner product [55]. The expansion coefficients can be determined by matching temperatures and heat fluxes at $\eta=0$ (regions 1 and 2) and at $\eta=\sigma/Pe$ (regions 2 and 3), where $\sigma\equiv L/r_0$ is the aspect ratio of the illuminated region. There are several methods [55–58] for actually computing the expansion coefficients, of which we have used that of Smith *et al.* [57]. The final formulae are

$$A_n=(1-e^{-\lambda_n\sigma/Pe})J_n$$

$$B_n=\begin{cases}-e^{-\lambda_n\sigma/Pe}J_n & n\leqslant -1\\ 0 & n=0\\ -J_n & n\geqslant 1\end{cases}$$

$$C_n=(e^{\lambda_n\sigma/Pe}-1)J_n$$

where

$$J_n=\frac{\int_0^1 H_n(\xi)[Pe^2(1-\xi^2)-\lambda_n]\theta_{fd}(\xi)\xi\,d\xi}{\int_0^1 H_n^2(\xi)[Pe^2(1-\xi^2)-2\lambda_n]\xi\,d\xi}. \tag{9}$$

To compute the integrals in (9), it has been necessary to recompute the eigenvalues λ_n and eigenfunctions $H_n(\xi)$ of (8a–c). Comparison to previous calculations at various Pe provided a check on our results, obtained by a shooting procedure employing a fourth-order Runge–Kutta method and a quasi-Newton iteration for the eigenvalues. The integrals in (9) were computed by Simpson's rule.

In practice, we truncate (6a–c) at a finite number of terms. Thus, we use

$$\theta_1(\xi,\eta)=\sum_{n=-N}^{-1}A_nH_n(\xi)\,e^{\lambda_n\eta}\qquad \eta<0$$

$$\theta_2(\xi,\eta)=\sum_{n=-N}^{N}B_nH_n(\xi)\,e^{\lambda_n\eta}+\theta_{fd}(\xi)\quad 0<\eta<\frac{\sigma}{Pe}$$

$$\theta_3(\xi,\eta)=\sum_{n=1}^{N}C_nH_n(\xi)\,e^{\lambda_n\eta}\qquad \frac{\sigma}{Pe}<\eta$$

with $5\leqslant N\leqslant 11$, according to the values of Pe, γ, and σ, in order to obtain results accurate to about 1%.

4. RESULTS

4.1. *Fully developed case*

For very long irradiated zones (large σ), the radial temperature distribution approaches a z-independent profile far downstream from the inlet to region 2. This profile is given by $\theta_{fd}(\xi)$ and is shown in Fig. 2 for several values of the optical density γ.

For small γ, it is easily seen from (7) that, to second order in γ, θ_{fd} approaches $(\gamma-\gamma^2)(1-\xi)$ as $\gamma\to 0$, an asymptotic behavior clearly displayed in Fig. 2. This almost linear dependence on ξ reflects the fact that at small γ there is very little attenuation of incident light; consequently, $1/\xi$ geometric focusing produces, in the limit $\gamma\to 0$, a situation wherein the light absorption rate per unit volume in an annular region between ξ and $\xi+\Delta\xi$ is independent of ξ. This leads to a nonzero value of $d\theta_{fd}/d\xi$ at $\xi=0$ and accounts for our specification of (8b) rather than the more familiar $dH_n(0)/d\xi=0$.

For larger γ, an increasingly large fraction of the light absorption occurs near the wall. This leads to, in the limit of large γ, very little transmission to the interior, and hence little opportunity for geometric focusing effects to be manifested in the temperature distribution. This is reflected in a progressive reduction of $d\theta_{fd}/d\xi$ along the centerline as γ increases.

Figure 3 shows the centerline (maximum) value of θ_{fd} as a function of γ. We observe that a maximum occurs for $\gamma=1.15$; for smaller γ, $\theta_{fd}(0)$ decreases due to reduced light absorption, while for larger γ, $\theta_{fd}(0)$

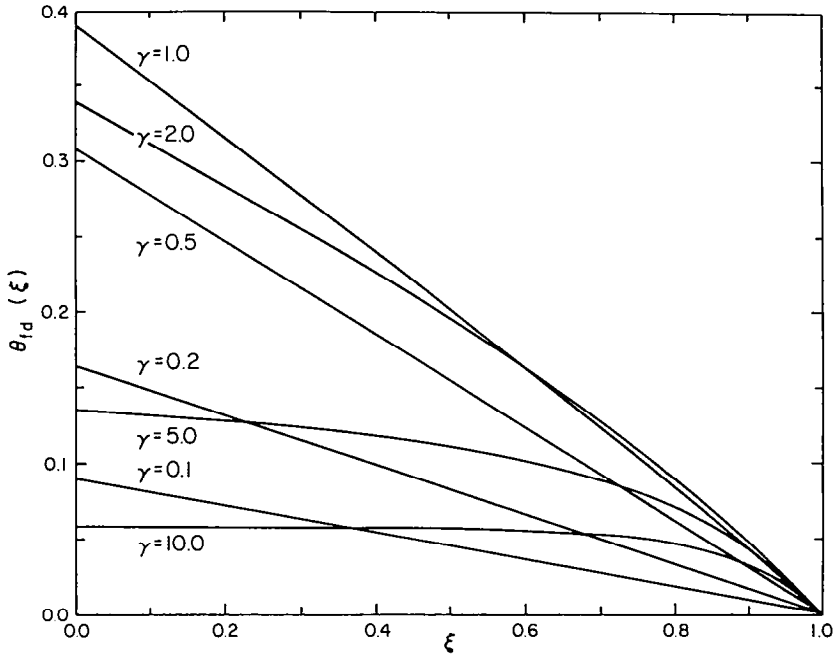

FIG. 2. Fully developed radial temperature profiles for various values of the optical density γ.

decreases due to increased absorption near the perfectly conducting (cold) wall at $\xi = 1$.

4.2. *Irradiated zone of finite length*

We begin with a discussion of the temperature distributions for $\sigma = 1$. This corresponds to a shorter illuminated region than that used in most of the previous experimental work [18–20, 43, 45, 48], but provides a useful illustration of the temperature distribution in an illuminated section of relatively small aspect ratio. Moreover, as discussed in Section 5, thermal considerations will frequently argue for using a number of short illuminated regions separated by dark zones, rather than a single longer illuminated region.

For a small value (1.0) of *Pe*, Fig. 4(a) shows that the maximum temperature θ_{max} occurs on the centerline, close to the center of the illuminated region

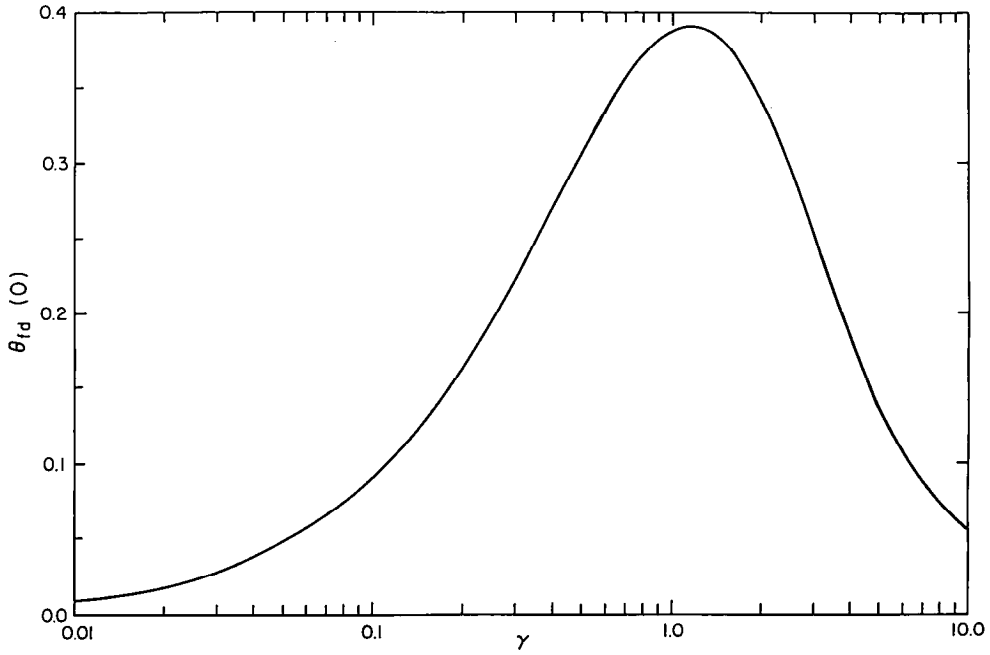

FIG. 3. Dimensionless centerline temperature of the fully developed profile as a function of γ.

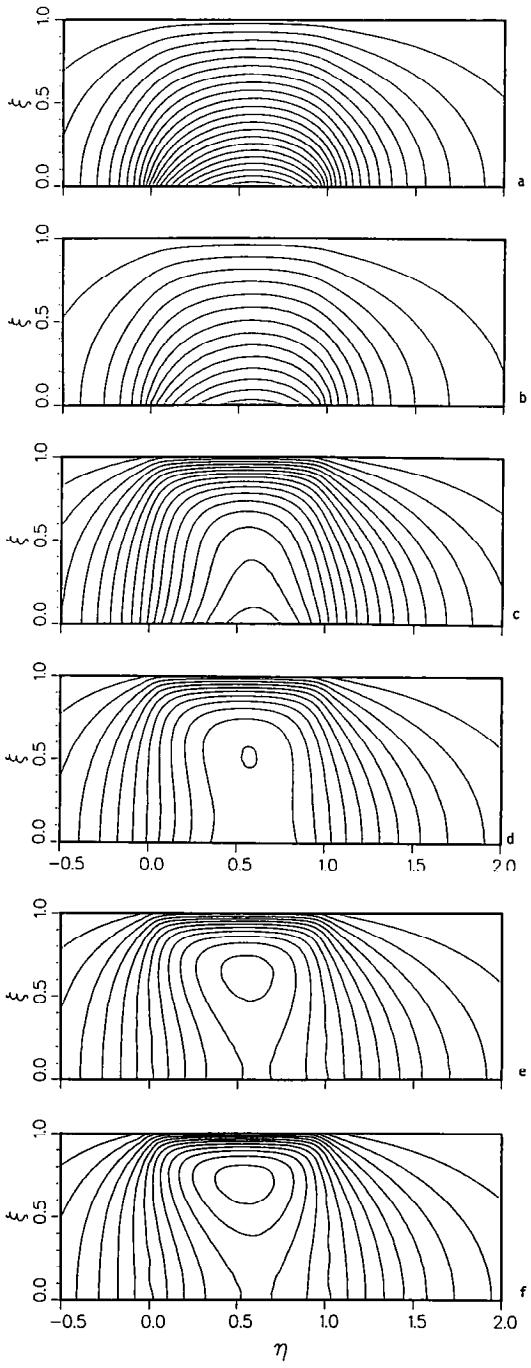

FIG. 4. Isotherms and hot spot temperatures θ_{hs} in the illuminated section ($0 \leqslant \eta \leqslant 1$) for $Pe = 1$, $\sigma = 1$, and various optical densities: (a) $\gamma = 0.1$, $\theta_{hs} = 0.068$, $\Delta\theta = 0.003$; (b) $\gamma = 1.0$, $\theta_{hs} = 0.291$, $\Delta\theta = 0.02$; (c) $\gamma = 5.0$, $\theta_{hs} = 0.088$, $\Delta\theta = 0.005$; (d) $\gamma = 6.5$, θ_{hs}(centerline) $= 0.0595$, $\theta_{hs}(\eta = 0.57, \xi = 0.50) = 0.0601$, $\Delta\theta = 0.005$; (e) $\gamma = 8.0$, $\theta_{hs} = 0.0494$, $\Delta\theta = 0.004$; (f) $\gamma = 10.0$, $\theta_{hs} = 0.0405$, $\Delta\theta = 0.003$.

for small γ (0.1). In Fig. 4(a), we see that the profile is an approximately linear function of ξ in the center of region 2. (Note that, by definition, the temperature at the wall is $\theta = 0$. The temperature difference between isotherms, $\Delta\theta$, is given separately for each figure.) This is not surprising, in light of the almost linear dependence of $\theta_{fd}(\xi)$ on ξ as $\gamma \to 0$, as discussed earlier. However, because of the relatively small value of σ (length/radius), the radial temperature profile does not approach $\theta_{fd}(\xi)$ anywhere in the tube. This accounts for the fact that the maximum temperature (on the centerline) is only about 0.068, rather than the fully developed value of 0.090. The approximate symmetry of the profile (about the plane $\eta = 0.5$) is due to the pronounced effect of axial conduction at this low value of Pe.

For $Pe = 1$ and $\sigma = 1$, Figs. 4(b) and (c) show that, as the optical density γ increases, the hot spot temperature initially increases (from 0.068 for $\gamma = 0.1$ to 0.29 for $\gamma = 1.0$) and then decreases (to 0.088 for $\gamma = 5.0$). This is due to the fact that, as γ increases, an increasing fraction of the absorbed light is absorbed close to the wall, to which heat is easily lost.

Figure 4(d) shows that, as γ increases to 6.5, a second hot spot forms away from the centerline. For still larger optical densities, Figs. 4(e) and (f) show that the centerline hot spot disappears and that the off-axis hot spot moves closer to the wall. This is accompanied by a continued reduction of the hot spot temperature (to 0.040 at $\gamma = 10.0$) as it moves closer to the cold ($\theta = 0$) wall. The approximate axial symmetry is due to the low value of Pe, and thus persists as γ increases.

For $Pe = 10$, Figs. 5(a)–(f) show a sequence of isotherms as γ is increased. For small γ (Fig. 5(a)) the temperature in the central portion of region 2 is an approximately linear function of radius (equally spaced isotherms), although the maximum centerline temperature (0.050) is still considerably below the fully developed value $\theta_{fd}(0) = \gamma = 0.1$, due to the shortness of section 2. We observe that for $Pe = 10$, there is much less axial symmetry (about $\eta = \sigma/(2Pe) = 0.05$) than in the $Pe = 1$ case, and the hot spot has shifted toward the downstream end of section 2. These effects are due to the reduced importance of axial conduction relative to convection.

As γ increases (Figs. 5(b) and (c)), a second hot spot forms away from the centerline. We note that this occurs via pinching and closure of isotherms, rather than via movement of the centerline hot spot away from the centerline. For $\gamma = 4.5$, we have $\theta = 0.063$ at the centerline hot spot, and $\theta = 0.059$ at the new one (near $\eta = 0.09$, $\xi = 0.5$). As γ increases, the temperatures of the two hot spots approach until at $\gamma = 4.9$ (Fig. 5(d)) the two hot spots have nearly the same temperature. For still larger γ, the maximum temperature occurs at the off-centerline hot spot (Fig. 5(e)). For sufficiently large γ (Fig. 5(f)), there is only one hot spot, which is off the centerline. In accordance with the previous discussion, the temperature at the off-centerline hot spot decreases as γ increases.

For $Pe = 30$, Figs. 6(a)–(d) show a similar sequence of isotherms and hot spot displacement as γ increases. This is close to the Pe above which axial conduction effects are likely to be unimportant except in a small

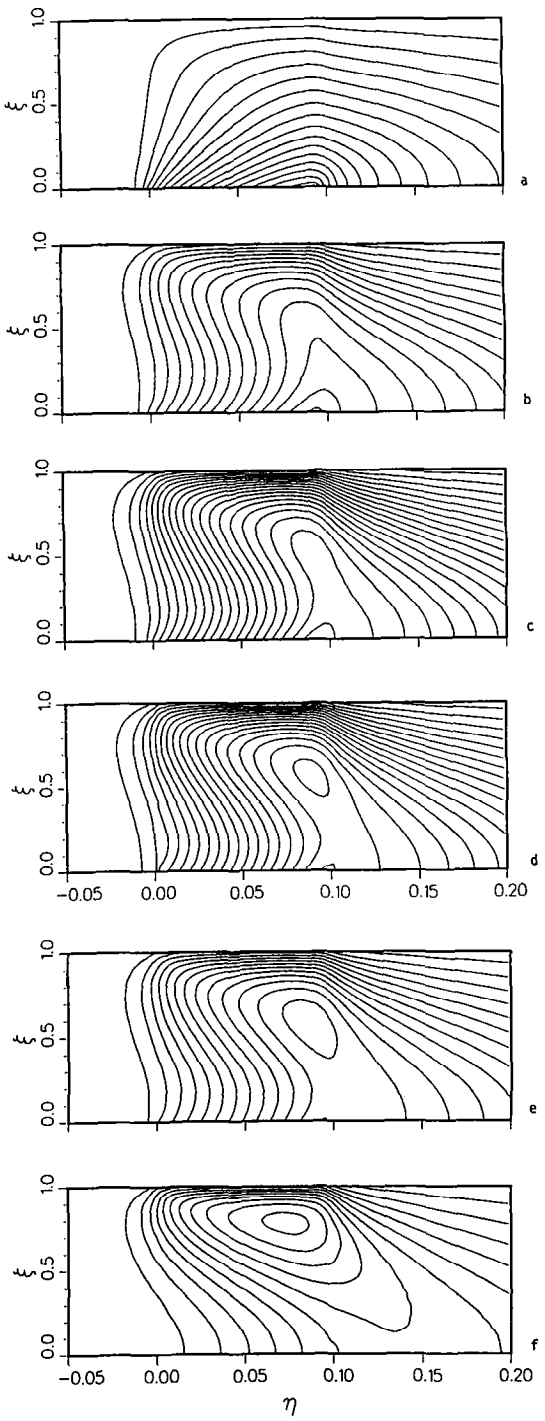

FIG. 5. Isotherms and hot spot temperatures θ_{hs} in the illuminated section ($0 \leqslant \eta \leqslant 0.1$) for $Pe = 10$, $\sigma = 1$, and various optical densities: (a) $\gamma = 0.1$, $\theta_{hs} = 0.0497$, $\Delta\theta = 0.003$; (b) $\gamma = 4.0$, $\theta_{hs} = 0.0766$, $\Delta\theta = 0.005$; (c) $\gamma = 4.5$, θ_{hs}(centerline) = 0.0630, $\theta_{hs}(\eta = 0.090, \xi = 0.48) = 0.0586$, $\Delta\theta = 0.003$; (d) $\gamma = 4.9$, θ_{hs}(centerline) = 0.0553, $\theta_{hs}(\eta = 0.088, \xi = 0.55) = 0.0549$, $\Delta\theta = 0.003$; (e) $\gamma = 5.0$, θ_{hs}(centerline) = 0.0531, $\theta_{hs}(\eta = 0.087, \xi = 0.57) = 0.0540$, $\Delta\theta = 0.004$; (f) $\gamma = 10.0$, $\theta_{hs} = 0.0336$, $\Delta\theta = 0.003$.

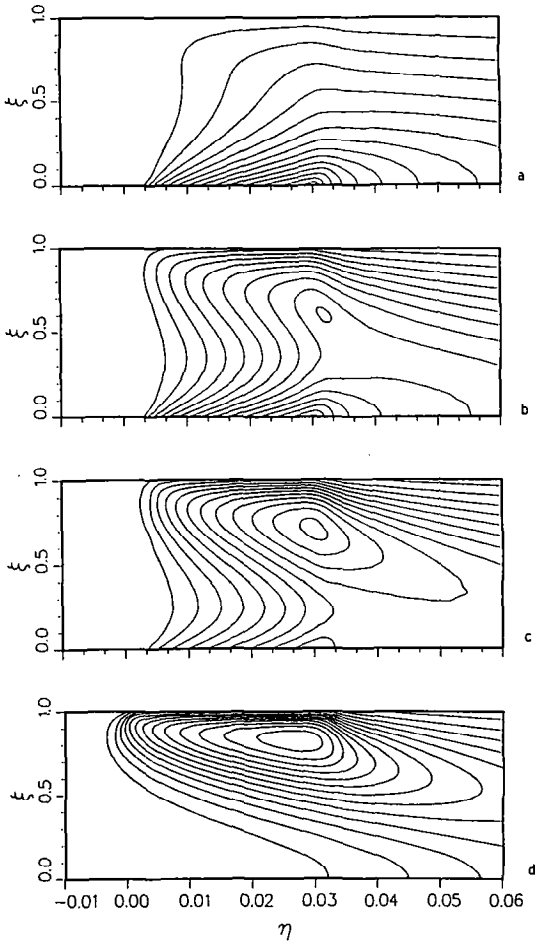

FIG. 6. Isotherms and hot spot temperatures θ_{hs} in the illuminated section ($0 \leqslant \eta \leqslant 0.0333$) for $Pe = 30$, $\sigma = 1$, and various optical densities: (a) $\gamma = 0.1$, $\theta_{hs} = 0.0299$, $\Delta\theta = 0.002$; (b) $\gamma = 2.8$, θ_{hs}(centerline) = 0.0618, $\theta_{hs}(\eta = 0.033, \xi = 0.56) = 0.0385$, $\Delta\theta = 0.003$; (c) $\gamma = 4.0$, θ_{hs}(centerline) = 0.0304, $\theta_{hs}(\eta = 0.032, \xi = 0.70) = 0.0368$, $\Delta\theta = 0.003$; (d) $\gamma = 10.0$, $\theta_{hs} = 0.0273$, $\Delta\theta = 0.002$.

region very close to the entrance [58]. In this regard we note that although entrance effects are still important (due to a relatively small σ), the isotherms near the exit of region 2 are relatively free of any influence of axial conduction. This reduced importance of axial conduction is further reflected in the fact that, as Pe increases, the hot spot moves closer to the downstream exit of the illuminated region.

A result having a less obvious explanation is that the maximum temperature (i.e. at the hot spot) decreases as Pe increases (compare the $Pe = 10$ and 30 results of Figs. 5(a) and 6(a) for $\gamma = 0.1$, Figs. 5(b) and 6(c) for $\gamma = 4.0$, and Figs. 5(f) and 6(d) for $\gamma = 10.0$). This is because, as shown previously [59], the thermal entry length increases with increasing Pe. Thus, for a tube having the relatively short aspect ratio $\sigma = L/r_0 = 1$, the temperature field is considerably less fully developed at the exit plane for $Pe = 30$ than for $Pe = 10$. Thus, θ at (or near) the exit plane should lie further below the fully developed value, consistent with the results. We will return to this point in connection with the $\sigma = 10$ results.

Figures 7(a)–(c) and 8(a)–(d) show isotherms for

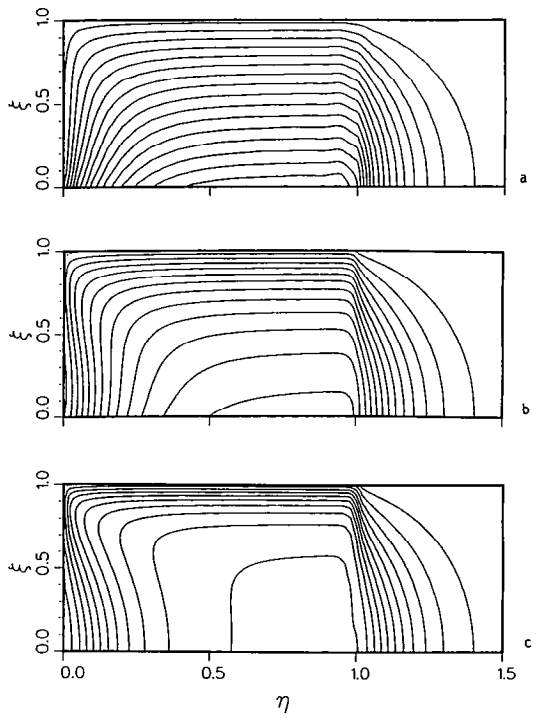

FIG. 7. Isotherms and hot spot temperatures θ_{hs} in the illuminated section ($0 \leqslant \eta \leqslant 1$) for $Pe = 10$, $\sigma = 10$, and various optical densities: (a) $\gamma = 2.0$, $\theta_{hs} = 0.338$, $\Delta\theta = 0.02$; (b) $\gamma = 5.0$, $\theta_{hs} = 0.135$, $\Delta\theta = 0.01$; (c) $\gamma = 10.0$, $\theta_{hs} = 0.0564$, $\Delta\theta = 0.005$.

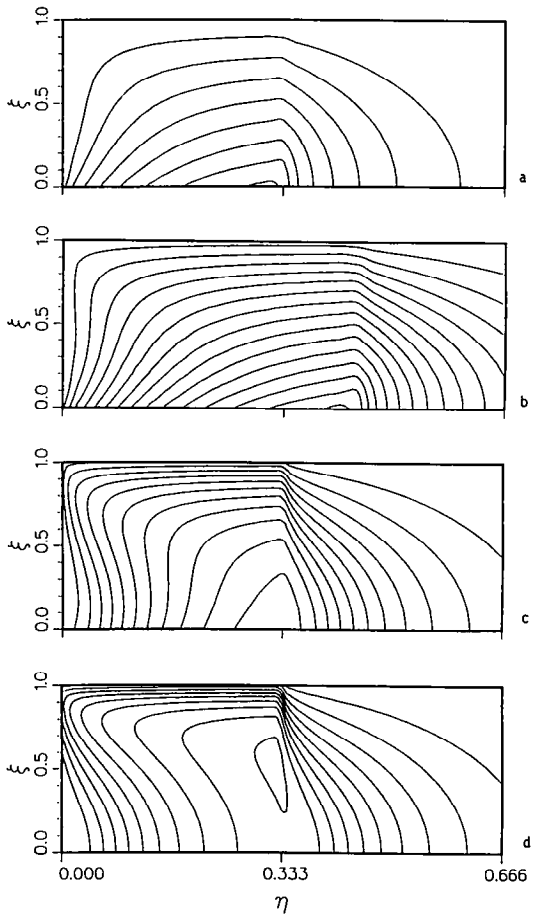

FIG. 8. Isotherms and hot spot temperatures θ_{hs} in the illuminated section ($0 \leqslant \eta \leqslant 0.333$) for $Pe = 30$, $\sigma = 10$, and various optical densities: (a) $\gamma = 0.1$, $\theta_{hs} = 0.0829$, $\Delta\theta = 0.01$; (b) $\gamma = 2.0$, $\theta_{hs} = 0.307$, $\Delta\theta = 0.02$; (c) $\gamma = 5.0$, $\theta_{hs} = 0.120$ $\Delta\theta = 0.01$; (d) $\gamma = 10.0$, θ_{hs}(centerline) = 0.0497, $\theta_{hs}(\eta = 0.32, \xi = 0.44) = 0.0508$, $\Delta\theta = 0.005$.

$\sigma = 10$. This aspect ratio is the same as that of the reactor used in the experiments of Cassano and Smith [45] and is similar to the aspect ratios (3.81 and 11.43) of the reactors employed by Dolan *et al.* [43], as well as the $\sigma = 20$ reactor of Matsuura *et al.* [20]. Figures 7(a)–(c) present results for $\sigma = 10$ and $Pe = 10$. The tubular reactor is illuminated for $0 \leqslant \eta \leqslant 1$. We first note that, in contrast to the $\sigma = 1$ results described earlier, the temperature distribution has become relatively fully developed in the central part ($0.4 \leqslant \eta \leqslant 0.9$) of the illuminated region upstream of the exit at $\eta = \sigma/Pe = 1$. For the range of γ studied (0.6–20), there is a single hot spot on the centerline. The effects of low Pe are manifested in the approximate symmetry of the isotherms about the center ($\eta = 0.5$) of the illuminated part of the tube, and in the location of the hot spot distinctly upstream of the exit plane, due to significant downstream conduction near $\eta = 1$.

For $Pe = 30$, Figs. 8(a)–(d) show an isotherm sequence as γ increases. The primary effect of increasing Pe is to reduce the importance of downstream axial conduction in the vicinity of the exit plane at $\eta = \sigma/Pe = 0.333$. Thus, the temperature distribution has considerably less upstream/downstream symmetry than for $Pe = 10$, and the centerline hot spots are much closer to the exit plane. We also note (compare Figs. 7(a) and 8(b) for $\gamma = 2.0$, Figs. 7(b) and 8(c) for $\gamma = 5.0$, and Figs. 7(c) and 8(d) for $\gamma = 10.0$) that the maximum temperatures are somewhat lower in the higher Pe case, as was earlier observed and discussed for the lower aspect ratio ($\sigma = 1$) tube. Finally, we note that the difference between the maximum temperatures for $Pe = 10$ and $Pe = 30$ is considerably smaller for $\sigma = 10$ than for the shorter tube ($\sigma = 1$) case. This is because the temperature distribution is considerably more fully developed for $\sigma = 10$, so that the localized effect of axial conduction in the vicinity of the exit plane is relatively more important for the higher σ case than for small σ, for which axial conduction was important everywhere in the flow.

The above points can be conveniently summarized in Table 1, where we show the maximum temperatures for several combinations of Pe and γ with $\sigma = 1$, 10, and ∞ (fully developed). The results clearly illustrate that the $\sigma = 10$ case is nearly fully developed for $Pe = 10$, is somewhat less fully developed for $Pe = 30$ (consistent with increasing thermal entry length as Pe increases), and that for $\sigma = 1$, the trend is similar,

Table 1. Maximum dimensionless temperature, θ

Pe	γ	$\sigma = 1$	$\sigma = 10$	$\sigma = \infty$ (fully developed)
10	5.0	0.0531 (0.0540)†	0.135	0.1354
	10.0	0.0336	0.0564	0.0566
30	0.1	0.0299	0.0829	0.0905
	2.0	0.0949	0.307	0.3385
	10.0	0.0273	0.0497 (0.0508)†	0.0566

† Quantities shown in parentheses are at off-centerline hot spots.

except that the temperature distribution is much less fully developed for both $Pe = 10$ and 30.

5. DISCUSSION

Our results show that for sufficiently small γ, the maximum temperature in a laminar flow tubular photoreactor occurs on the centerline. For sufficiently large optical densities, the maximum temperature occurs at a hot spot away from the centerline. For intermediate values of the optical density, there may be two local hot spots. The results thus show that the off-centerline hot spot develops independently of that on the centerline and does not result from movement of the centerline hot spot.

The results also show, as might be expected, that for $\sigma = 1$, the temperature distribution does not approach a fully developed profile anywhere in region 2 for any Pe and γ examined. This may be significant in minimizing the maximum temperature in the reactor, an objective that will usually be desirable for the reasons discussed in Section 1. Thus, in a given situation, it may be desirable to divide the reactor into a number, say M, of illuminated regions separated by $M-1$ unilluminated interstage cooling sections. If the lengths of the irradiated and unirradiated regions are properly chosen, the fluid will have sufficient residence time between illuminated zones to lose its excess heat to the tube wall, thus resulting in a lower maximum temperature than would be possible with a single irradiated zone of equivalent length.

Upstream displacement of the hot spot(s) from the exit plane of the illuminated zone (Section 2) is, as might be expected, more pronounced at lower Pe, for which axial conduction is more important. We also note for both small γ (Figs. 4(a), 5(a) and 6(a) for $\gamma = 0.1$) and large γ (Figs. 4(b), 5(f), and 6(d) for $\gamma = 10.0$), the maximum temperature is a decreasing function of Pe. This is because our (standard) nondimensionalization gives $\eta_{exit} = \sigma/Pe$, so that as Pe increases, the dimensionless length of region 2 decreases, resulting in a radial temperature profile that is less fully developed as Pe increases. For the Pe shown, this effect is more important than axial conduction, which tends to reduce the maximum temperature in addition to displacing the hot spot upstream from the exit.

Deciding whether centerline or off-centerline hot spots are more deleterious in a given situation will typically depend on several factors. If thermal decomposition of the reactant(s) or sensitizer is important, then thermal control everywhere is important, owing to the nature of the mass flow rate distribution for a parabolic velocity profile. If, however, thermal decomposition of the desired product is to be avoided, then the maximum temperature near the tube wall will be especially important for high optical density, in which case light absorption (and product formation) is concentrated close to the tube wall.

REFERENCES

1. D. R. Arnold and P. de Mayo, Photochemistry and industry, *Chemtech* 615–620 (1971).
2. J. M. Mellor, D. Phillips and K. Salisbury, Photochemistry: new technological applications, *Chem. Britain* **10**(5), 160–175 (1974).
3. M. Fischer, Industrial applications of photochemical syntheses, *Angew. Chem. Int. Ed. Engl.* **17**, 16–26 (1978).
4. J. J. Bloomfield and D. C. Owsley, Photochemical technology. In *Kirk-Othmer Encyclopedia of Chemical Technology* (3rd Edn), Vol. 17, (Edited by M. Grayson). Wiley, New York (1982).
5. K. H. Ploertner, Photochemistry in industrial synthesis, *J. Photochem.* **25**, 91–97 (1984).
6. M. T. Suidan and B. F. Severin, Light intensity models for annular UV disinfection reactors, *A.I.Ch.E. Jl* **32**, 1902–1909 (1986).
7. A. Roloff, K. Meier and M. Riediker, Synthetic and metal organic photochemistry in industry, *Pure Appl. Chem.* **58**, 1267–1272 (1986).
8. G. Terrones and A. J. Pearlstein, Absorbance, light intensity, mass transfer, and sampling time effects in a proposed mechanism for the photolysis of phenyl azide, *J. Am. Chem. Soc.* **113**, 2132–2140 (1991).
9. A. J. Pearlstein, Criteria for the absence of thermal convection in photochemical systems, *J. Phys. Chem.* **89**, 1054–1058 (1985).
10. J. G. Calvert and J. N. Pitts, *Photochemistry*. Wiley, New York (1966).
11. A. E. Cassano, P. L. Silveston and J. M. Smith, Photochemical reaction engineering, *Ind. Eng. Chem.* **59**(1), 18–38 (1967).
12. R. T. Bailey and F. R. Cruickshank, Infrared emission of low pressure gases induced by carbon dioxide laser radiation, *J. Phys. Chem.* **80**, 1596–1601 (1976).
13. J. C. Andre, M. L. Viriot, J. Villermaux and A. Tournier, Pourquoi pas des reactions photochemiques industrielles, *Entropie* **107–108**, 62–81 (1982).
14. O. M. Alfano, R. L. Romero and A. E. Cassano, Radiation field modelling in photoreactors—I: Homogeneous media, *Chem. Eng. Sci.* **41**, 421–444 (1986).
15. U.-W. Grummit, H. Langbein, R. Noske and G. Robisch, Photochromism and thermochromism of dithizone in solution, *J. Photochem.* **27**, 249–257 (1984).
16. T. Hutson and R. S. Logan, Development of a photochlorination reactor, *Chem. Eng. Prog.* **68**(5), 76–77 (1972).
17. W. T. Anderson, Photosensitization in chlorination, *Ind. Eng. Chem.* **39**, 844–846 (1947).
18. C. A. Walker and F. C. Baginski, Photochemical reaction of hydrogen sulfide with n-octene-1, *Chem. Eng. Prog. Symp. Ser.* **62**(68), 38–46 (1966).
19. D. Ziolkowski, A. E. Cassano and J. M. Smith, Effect

of wall deposit on photochlorination kinetics, *A.I.Ch.E. Jl* **13,** 1025–1028 (1967).
20. T. Matsuura, A. E. Cassano and J. M. Smith, Acetone photolysis: kinetic studies in a flow reactor, *A.I.Ch.E. Jl* **15,** 495–501 (1969).
21. R. S. Davidson, Practical aspects of photochemistry, *Chemistry and Industry* 180–193 (1978).
22. A. D. Clements, Photochemistry in commercial synthesis, *Chem. Britain* **16,** 464–467 (1980).
23. J. B. Biddle, D. B. Peterson and T. Fujita, *Solar Photochemical Process Engineering for Production of Fuels and Chemicals.* NASA CR-173910, Jet Propulsion Laboratory, Pasadena, California (1984).
24. D. B. Peterson, J. R. Biddle and T. Fujita, *Review of Solar Fuel-producing Quantum Conversion Processes.* NASA CR-173904, Jet Propulsion Laboratory, Pasadena, California (1984).
25. L. R. Evans and R. E. Neligan, Vapor-phase chlorination of dimethyl ether, *Ind. Eng. Chem.* **52,** 379–380 (1960).
26. F. Chen and A. J. Pearlstein, Temperature distributions in a laminar-flow tubular photoreactor, *A.I.Ch.E. Jl* **34,** 1381–1383 (1988).
27. R. M. Noyes, Wall effects in photochemically induced chain reactions, *J. Am. Chem. Soc.* **73,** 3039–3043 (1951).
28. R. M. Noyes, Photochemical space intermittency; a proposal for measuring diffusion coefficients of reactive free radicals, *J. Am. Chem. Soc.* **81,** 566–570 (1959).
29. G. A. Salmon and R. M. Noyes, Evidence for photochemical space intermittency effect, *J. Am. Chem. Soc.* **84,** 672–673 (1962).
30. S. A. Levison and R. M. Noyes, Diffusion coefficients of iodine atoms in carbon tetrachloride by photochemical space intermittency, *J. Am. Chem. Soc.* **86,** 4525–4529 (1964).
31. R. D. Burkhart, R. F. Boynton and J. C. Merrill, Studies on diffusion and diffusion-controlled reactions involving alkyl radicals in solution, *J. Am. Chem. Soc.* **93,** 5013–5017 (1971).
32. A. C. Muller, J. C. Eichacker and F. B. Hill, *The Effects of Partial Illumination and Mixing on the Sensitized Photopolymerization of Methyl Methacrylate,* BNL 16455, Brookhaven National Laboratory, Brookhaven, New York (1971).
33. J. P. Laplante and R. J. Pottier, Study of the oscillatory behavior in irradiated 9,10-dimethylanthracene/chloroform solutions, *J. Phys. Chem.* **86,** 4759–4766 (1982).
34. I. R. Epstein, M. Morgan, C. Steel and O. Valdes-Aguilera, Biacetyl-oxygen and other photochemical oscillators: the role of hydrodynamically induced instability, *J. Phys. Chem.* **87,** 3955–3958 (1983).
35. J. C. Micheau, M. Gimenez, P. Borckmans and G. Dewel, Hydrodynamic instability and photochemical reactions, *Nature* **305,** 43–45 (1983).
36. D. Avnir and M. Kagan, Spatial structures generated by chemical reactions at interfaces, *Nature* **307,** 717–720 (1984).
37. J. P. Laplante, J. C. Micheau and M. Gimenez, Oscillatory fluorescence in irradiated solutions of 9,10-dimethylanthracene in chloroform. A probe for convective motion? *J. Phys. Chem.* **88,** 4135–4137 (1984).
38. S. Ruschin and S. H. Bauer, Oscillating convective effects in SF_6–Ar laser-heated mixtures, *J. Phys. Chem.* **88,** 5042–5048 (1984).
39. E. C. Zimmermann and J. Ross, Light induced bistability in $S_2O_6F_2 \rightleftharpoons 2SO_3F$: theory and experiment, *J. Chem. Phys.* **80,** 720–729 (1984).
40. M. Gimenez, J. C. Micheau, D. Lavabre and J. P. Laplante, Oscillatory convective behavior and fluorescence analysis, *J. Phys. Chem.* **89,** 1–5 (1985).
41. F. Santarelli, C. Stramigioli, G. Spiga and M. N. Ozisik, Effects of scattering and reflection of radiation on batch photochemical reaction in a slab geometry, *Int. J. Heat Mass Transfer* **25,** 57–62 (1982).
42. R. S. Schechter and E. H. Wissler, Photochemical reactions in an isothermal laminar-flow chemical reactor, *Appl. Sci. Res.* **9A,** 334–344 (1960).
43. W. J. Dolan, C. A. Dimon and J. S. Dranoff, Dimensional analysis in photochemical reactor design, *A.I.Ch.E. Jl* **11,** 1000–1005 (1965).
44. F. B. Hill and R. M. Felder, Effects of mixing on chain reactions in isothermal photoreactors, *A.I.Ch.E. Jl* **11,** 873–885 (1965).
45. A. E. Cassano and J. M. Smith, Photochlorination in a tubular reactor, *A.I.Ch.E. Jl* **12,** 1124–1133 (1966).
46. Y. Harano and J. M. Smith, Tubular flow photoreactors for complex, nonchain kinetics, *A.I.Ch.E. Jl* **14,** 584–591 (1968).
47. F. B. Hill, N. Reiss and L. H. Shendalman, Nonuniform initiation of photoreactions. III. Reactant diffusion in single-step reactions, *A.I.Ch.E. Jl* **14,** 798–804 (1968).
48. W. J. Zolner and J. A. Williams, The effect of angular light intensity distribution on the performance of tubular flow photoreactors, *A.I.Ch.E. Jl* **18,** 1189–1195 (1972).
49. D. Brkic, P. Forzatti and F. Trifico, The photosensitized oxygenation of olefins with reactors of different types, *Chem. Eng. Sci.* **33,** 853–861 (1978).
50. L. H. Shendalman and F. B. Hill, Mixing effects, optimisation, and dispersion modelling in bleachable and sensitised photoreaction mixtures, *Chem. Eng. J.* **2,** 261–273 (1971).
51. S. K. Mendiratta, R. M. Felder and F. B. Hill, Benzoin- and benzoin methyl ether-sensitized photopolymerization of styrene and methyl methacrylate: quantum yields and mixing effects, *A.I.Ch.E. Jl* **21,** 1115–1123 (1975).
52. M. Koizumi and T. Matsuura, *Photosensitized Reactions.* Kagakudojin Publishing Co., Kyoto (1978). (In English.)
53. R. B. Bird, W. E. Stewart and E. N. Lightfoot, *Transport Phenomena.* Wiley, New York (1960).
54. C.-J. Hsu, An exact analysis of low Peclet number thermal entry region heat transfer in transversely nonuniform velocity fields, *A.I.Ch.E. Jl* **17,** 732–740 (1971).
55. A. J. Pearlstein, Exact, efficient calculation of coefficients in certain eigenfunction expansions, *Appl. Sci. Res.* **30,** 337–340 (1975).
56. E. Papoutsakis, D. Ramkrishna and H. C. Lim, The extended Graetz problem with Dirichlet wall boundary conditions, *Appl. Sci. Res.* **36,** 13–34 (1980).
57. C. E. Smith, M. Faghri and J. R. Welty, On the determination of temperature distribution in laminar pipe flow with a step change in wall heat flux, *J. Heat Transfer* **97,** 137–139 (1975).
58. E. Papoutsakis, D. Ramkrishna and H. C. Lim, The extended Graetz problem with prescribed wall flux, *A.I.Ch.E. Jl* **26,** 779–787 (1980).
59. P. J. Schneider, Effects of axial fluid conduction on heat transfer in the entrance regions of parallel plates and tubes, *Trans. ASME* **79,** 765–773 (1957).